Room-temperature fabrication of defective CoO_xH_y nanosheets with abundant oxygen vacancies and high porosity as efficient 5-hydroxymethylfurfural oxidation electrocatalysts

Ruyi Zhong[a], Puwei Wu[a], Qi Wang[b], Xiting Zhang[a], Lei Du[a], Yunhua Liu[a], Huakang Yang[a], Meng Gu[b], Z. Conrad Zhang[c], Limin Huang[d,], and Siyu Ye[a,]**

[a]Huangpu Hydrogen Energy Innovation Center/Guangzhou Key Laboratory for Clean Energy and Materials, School of Chemistry and Chemical Engineering, Guangzhou University, Guangzhou 510006, P.R. China.

[b]Department of Materials Science and Engineering, Southern University of Science and Technology, Shenzhen 518055, P.R. China.

[c]Dalian National Laboratory for Clean Energy, Dalian Institute of Chemical Physics, Chinese Academy of Sciences, Dalian 116023, P.R. China.

[d]Department of Chemistry, Southern University of Science and Technology, Shenzhen 518055, P.R. China.

* Corresponding author: huanglm@sustech.edu.cn (L.-M. Huang); siyu.ye@gzhu.edu.cn (S. Ye)

Table S1. The fitted parameters of Nyquist plots of CoO_xH_y, CoO_xH_y-MA, CoO_xH_y-BH, and CoO_xH_y-MA/BH.

Catalyst	R_s (Ω)	R_{ct} (Ω)	CPE-T (F)	CPE-P
CoO_xH_y	11.6	36.7	0.0006	0.80
CoO_xH_y-MA	10.9	8.1	0.0035	0.88
CoO_xH_y-BH	10.9	15.1	0.0026	0.77
CoO_xH_y-MA/BH	12.6	11.1	0.0022	0.81

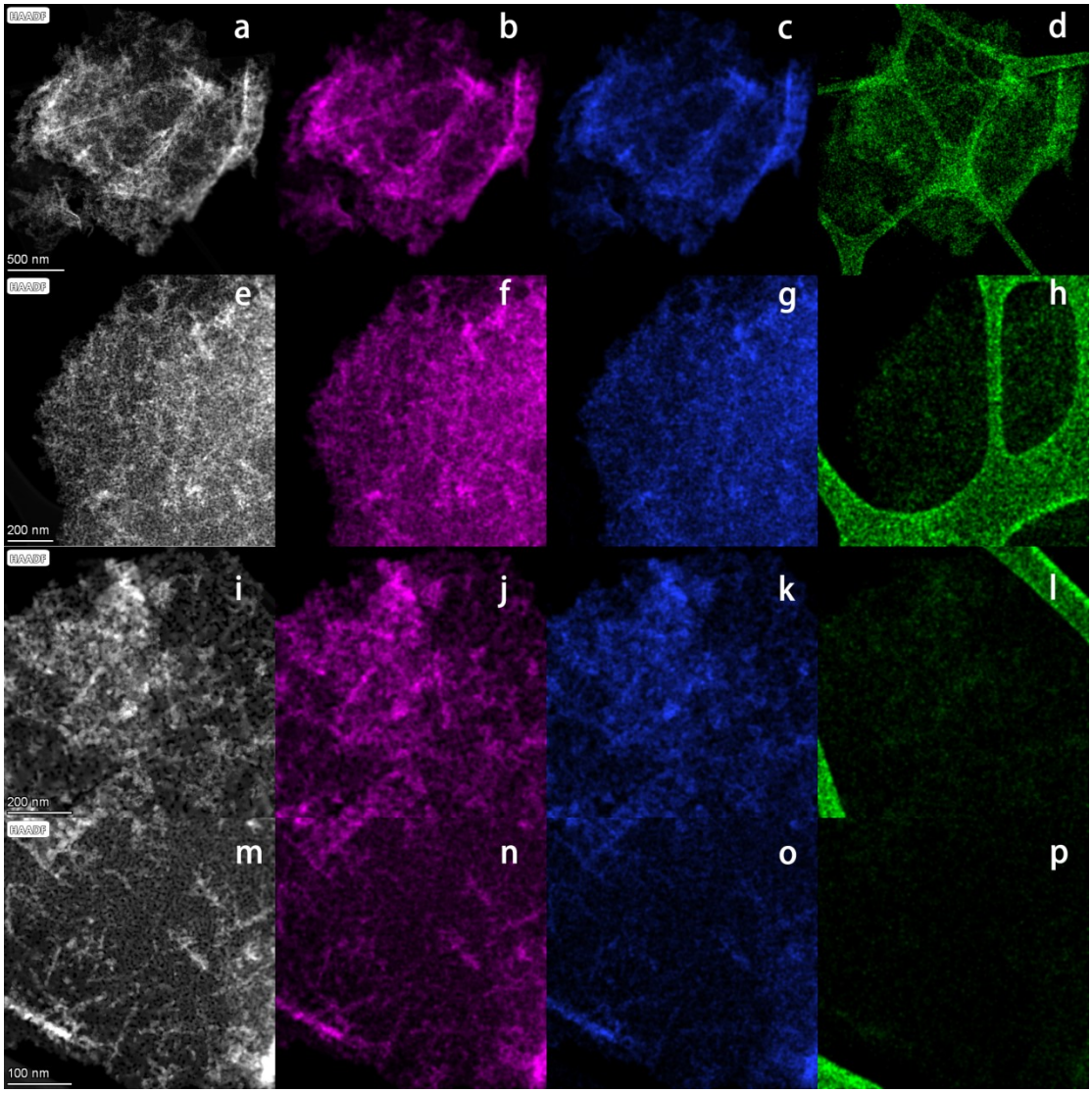

Figure S1. (a, e, i, m) The HAADF-STEM images, and the corresponding EDS mappings of (b-d) Co_3O_4-300, (f-h) Co_3O_4-300-MA, (j-l) Co_3O_4-300-BH, and (n-p) Co_3O_4-300-MA/BH. The Co, O, and C elements were represented in the color of magenta, blue, and green, respectively.

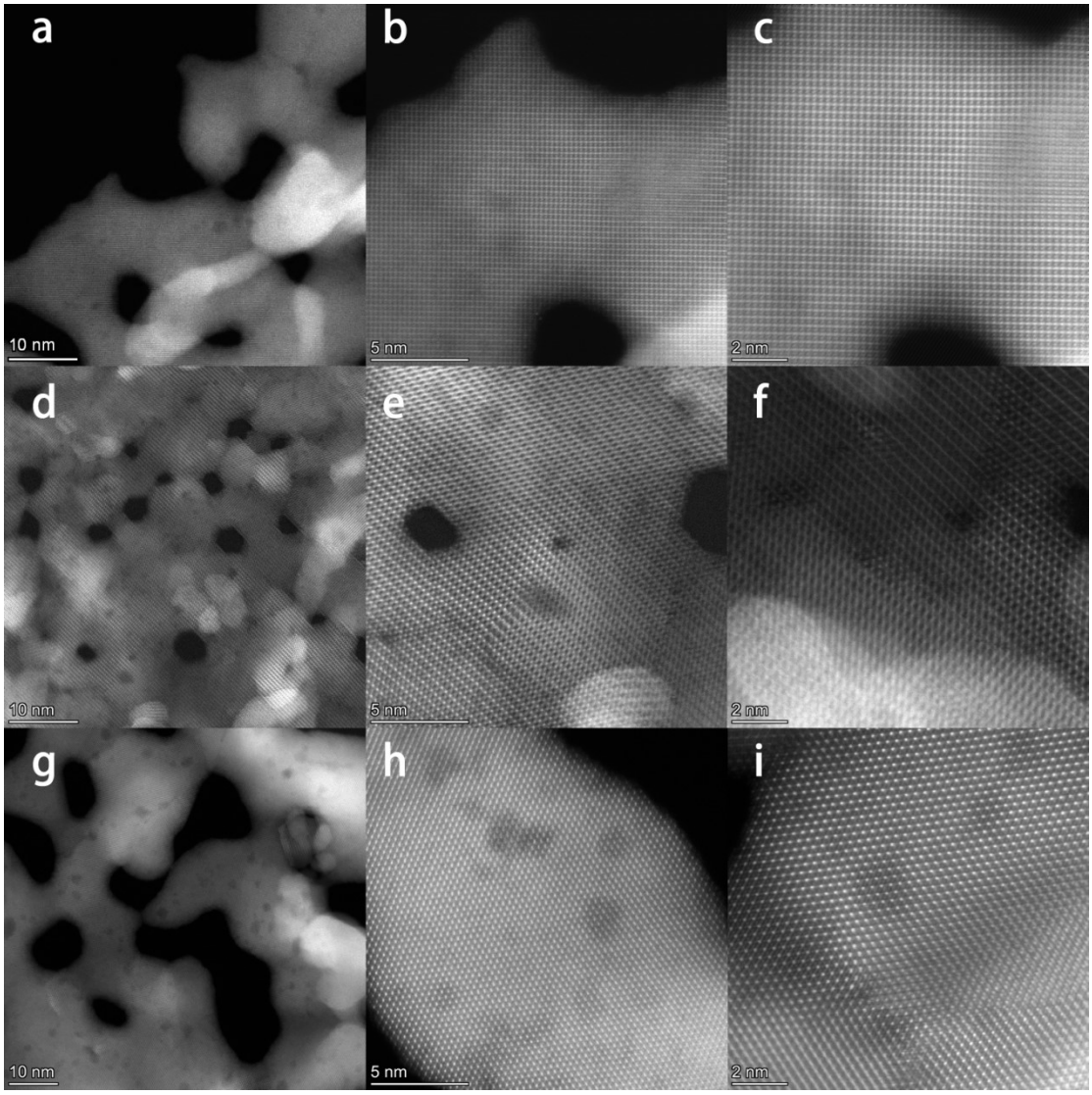

Figure S2. HRTEM images with increased magnifications of (a-c) Co_3O_4-300-MA, (d-f) Co_3O_4-300-MA, and (g-i) Co_3O_4-300-MA/BH.

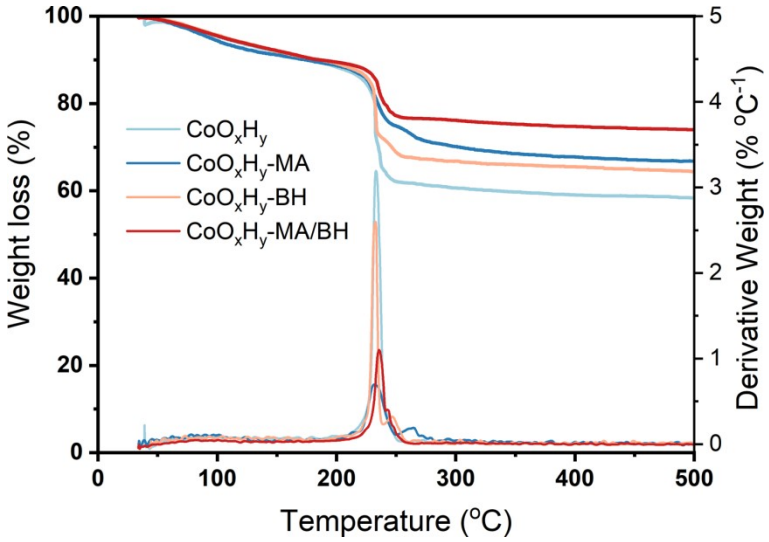

Figure S3. TGA/DTG profiles of CoO_xH_y, CoO_xH_y-MA, CoO_xH_y-BH, and CoO_xH_y-MA/BH.

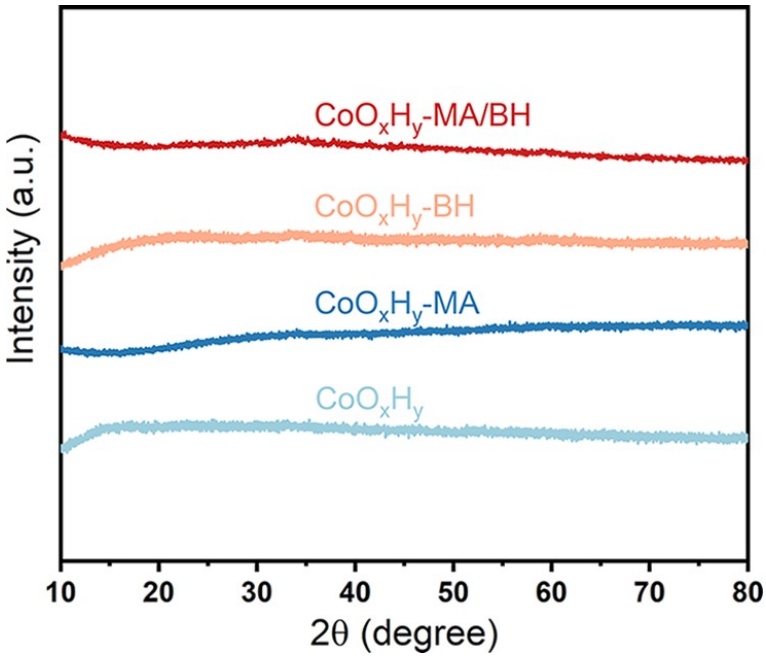

Figure S4. XRD patterns of CoO_xH_y, CoO_xH_y-MA, CoO_xH_y-BH, and CoO_xH_y-MA/BH.

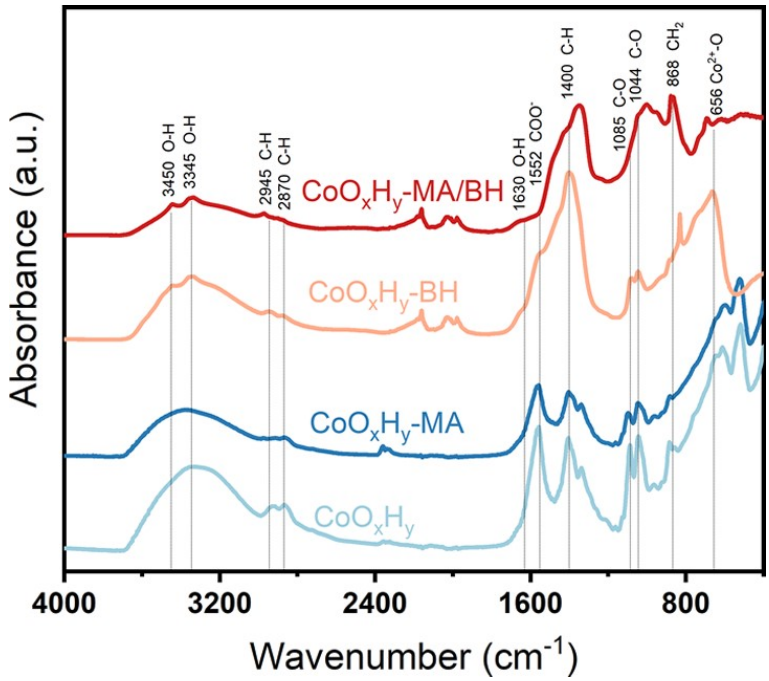

Figure S5. FTIR spectra of CoO_xH_y, CoO_xH_y-MA, CoO_xH_y-BH, and CoO_xH_y-MA/BH.

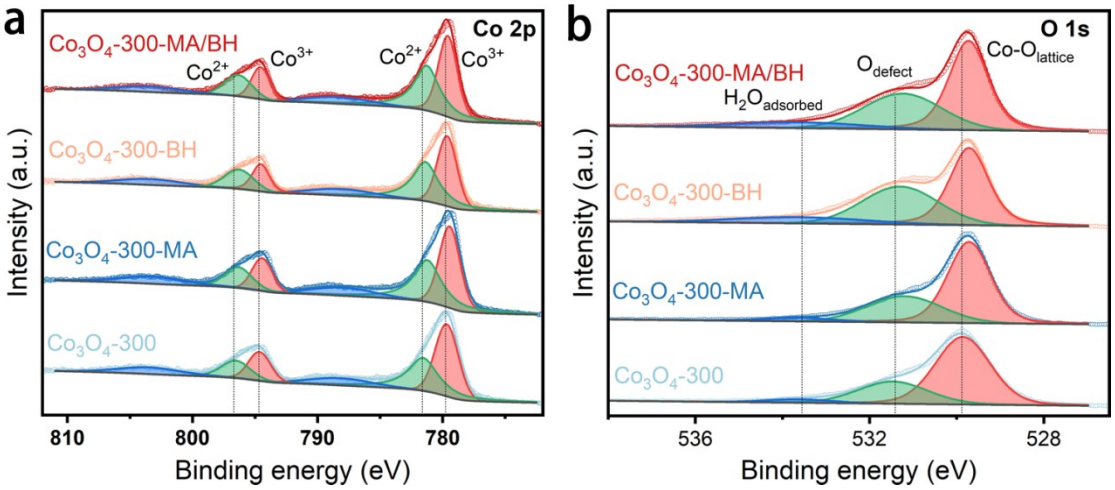

Figure S6. XPS (a) Co 2p and (b) O 1s spectra of Co_3O_4-300, Co_3O_4-300-MA, Co_3O_4-300-BH, and Co_3O_4-300-MA/BH.

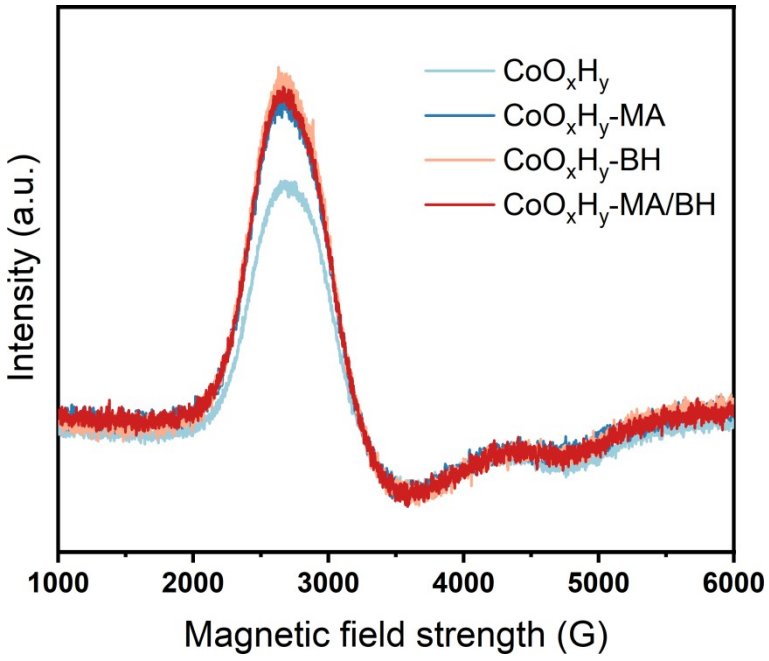

Figure S7. EPR signals against magnetic field strength of CoO_xH_y, CoO_xH_y-MA, CoO_xH_y-BH, and CoO_xH_y-MA/BH.

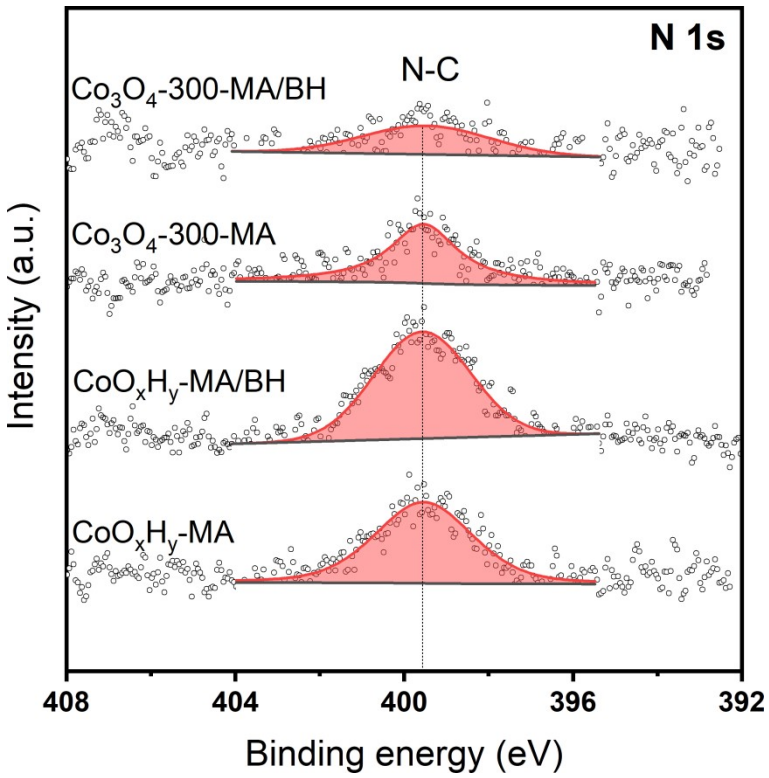

Figure S8. XPS N 1s spectra of CoO_xH_y-MA, CoO_xH_y-MA/BH, Co_3O_4-300-MA, and Co_3O_4-300-MA/BH.

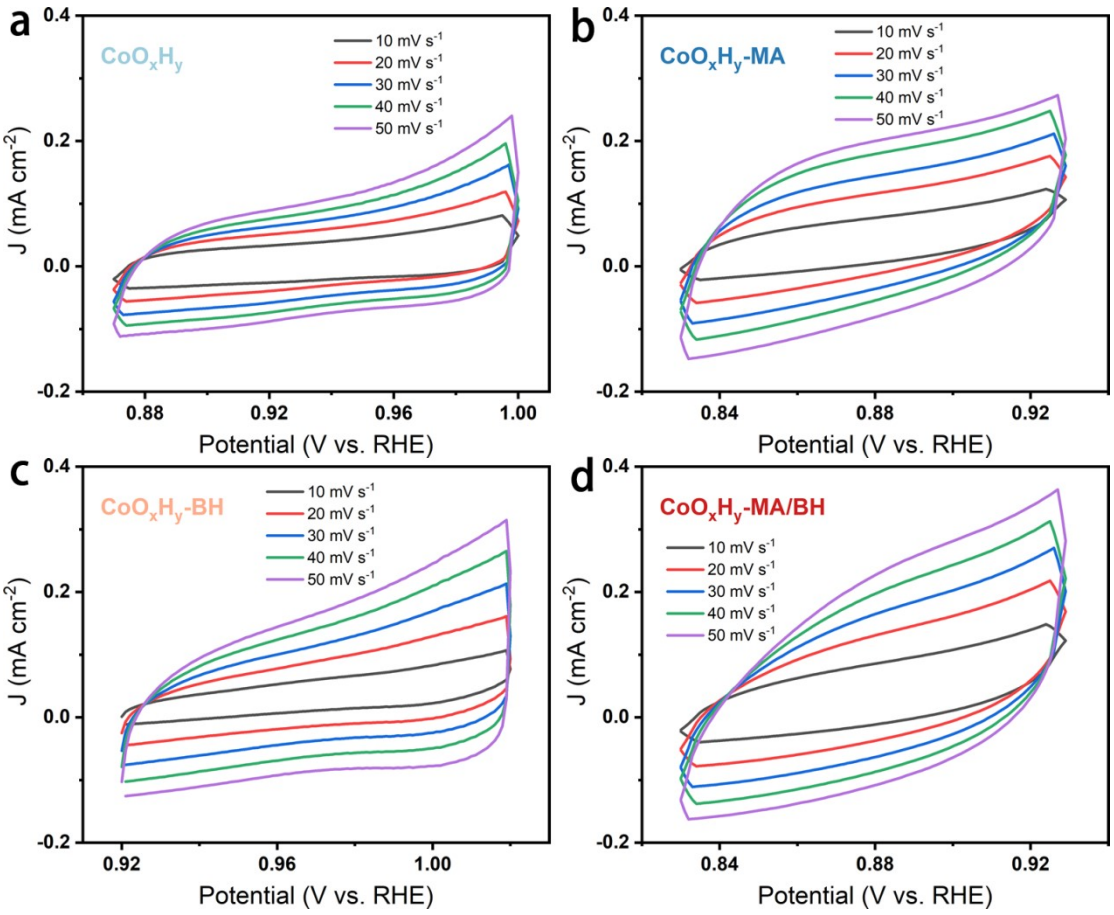

Figure S9. CVs at different scanning rates from 10 to 50 mV s^{-1} of (a) CoO_xH_y, (b) CoO_xH_y-MA, (c) CoO_xH_y-BH, and (d) CoO_xH_y-MA/BH.

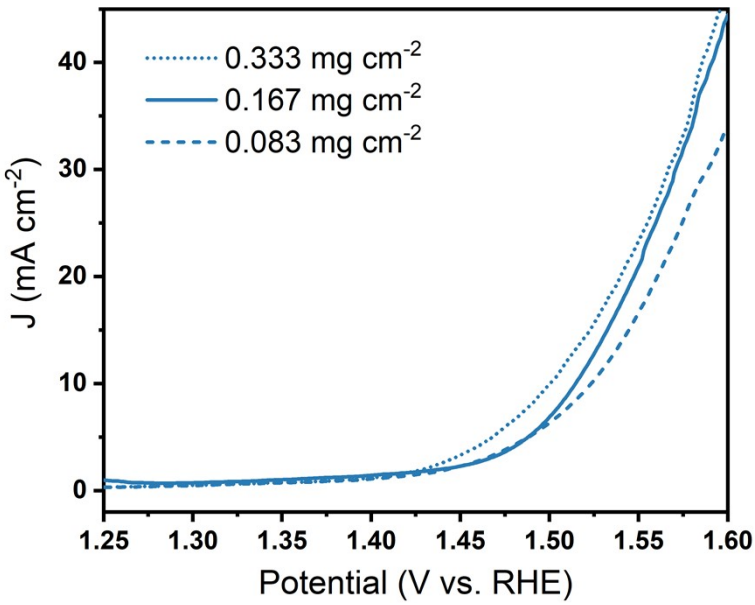

Figure S10. The HMFOR LSVs of CoO_xH_y-MA with different loadings on the glassy carbon electrode in 1 M KOH solution containing 5 mM HMF at a scanning rate of 5 mV s^{-1}.

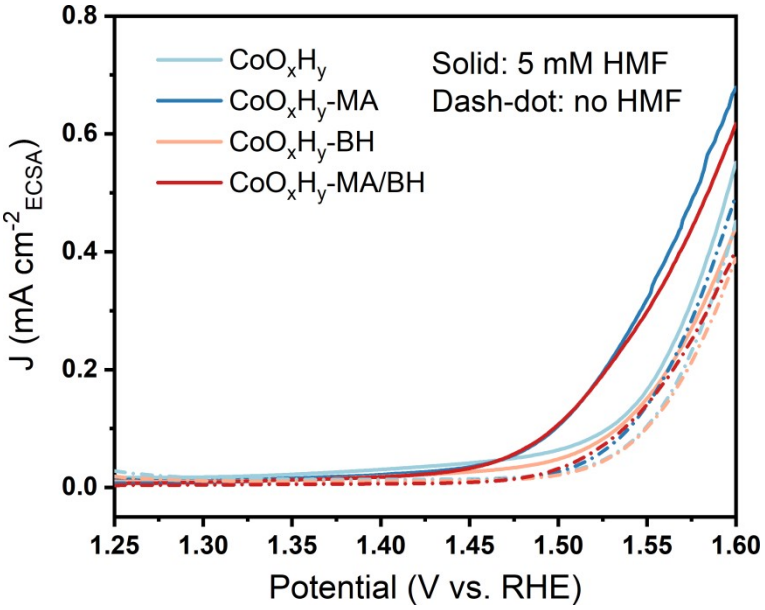

Figure S11. The HMF and OER performance of CoO_xH_y, CoO_xH_y-MA, CoO_xH_y-BH, and CoO_xH_y-MA/BH after normalization to their electrochemical surface area.

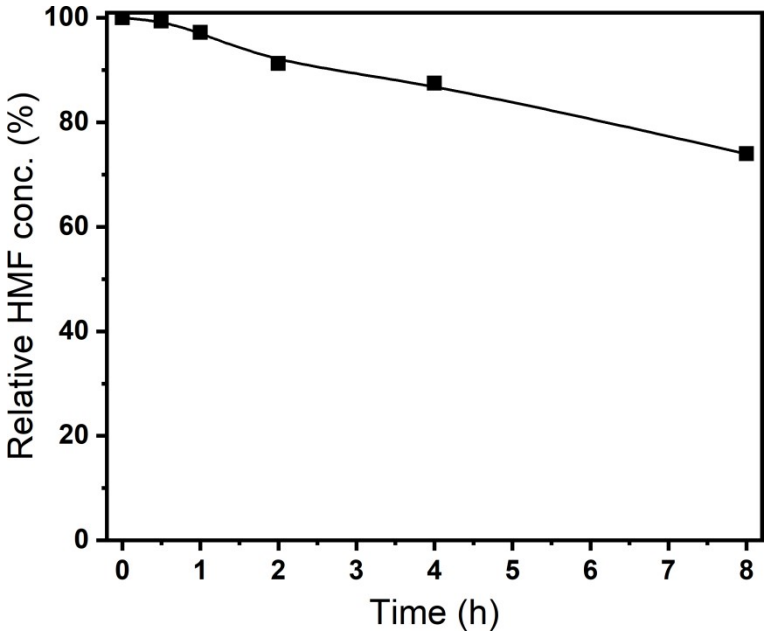

Figure S12. HMF thermodegradation of 5 mM HMF in 1 M KOH without electrocatalysts.

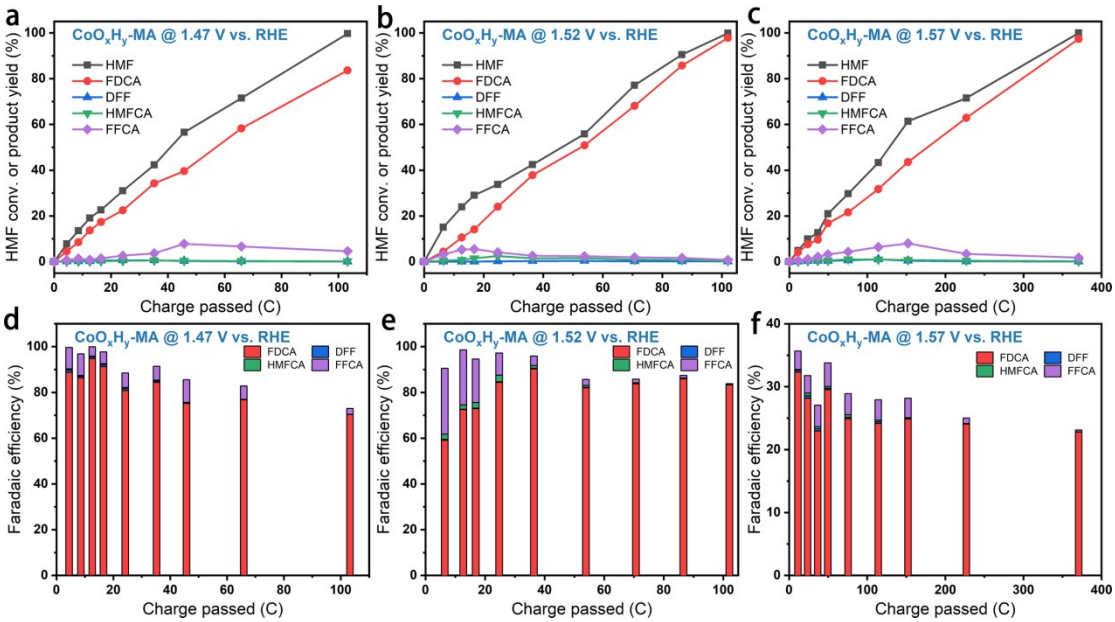

Figure S13. (a, b, c) The conversion of HMF and the yields of oxidation products, and (d, e, f) the corresponding Faradaic efficiency of CoO_xH_y-MA in 1.0 M KOH containing 5 mM HMF at different potentials of (a, d) 1.47, (b, e) 1.52, and (c, f) 1.57 V, respectively.

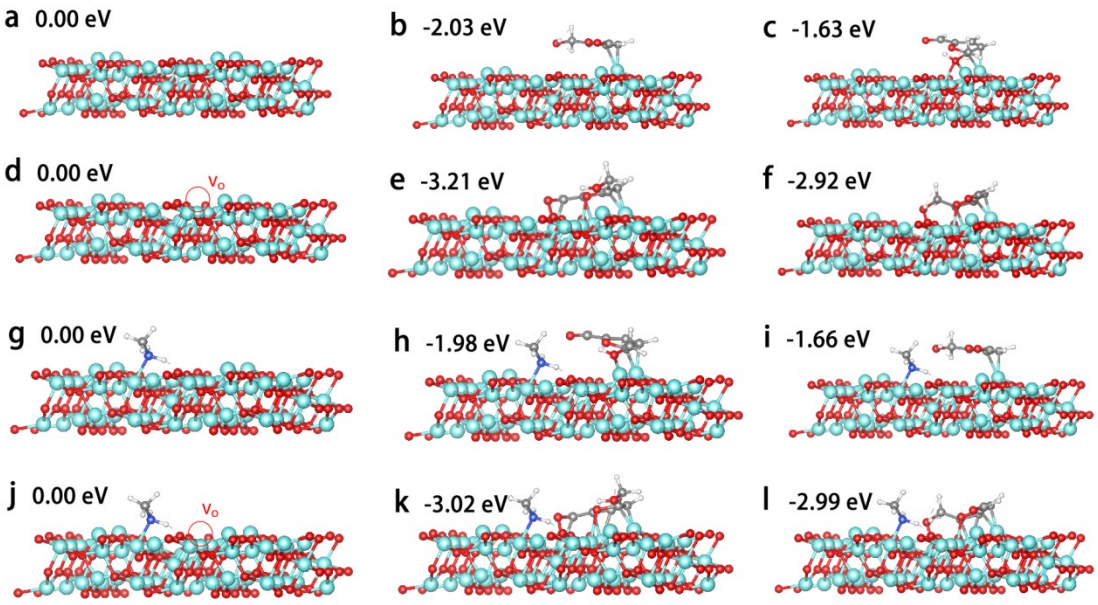

Figure S14. DFT-calculated adsorption configurations for Co_3O_4 catalysts: (a, b, c) (3 1 1) surface, (d, e, f) in the presence of surface oxygen vacancy (V_O) site, (g, h, i) in the presence of chemisorbed methylamine (MA) molecule, and (j, k, l) in the presence of V_O and MA. (b, d, g, j) represent the adsorption behavior of HMF starting from its -CHO group, and (c, f, i, l) represent the adsorption behavior of HMF starting from its -C-OH group.